Quasistatic fracture evolution using a nonlocal cohesive model

Debdeep Bhattacharya ⓘ · **Robert Lipton** ⓘ ·
Patrick Diehl ⓘ

Abstract We introduce a nonlocal model of peridynamic type for fracture evolution in the quasistatic regime. Nonlocal quasistatic fracture evolution is developed and supporting numerical examples are presented. The approach is implicit and is based on local stationary and fixed point methods. Here a smooth cohesive force-strain model is used. Initially the force increases with strain then softens and decreases to zero. It is proved that the fracture evolution decreases stored elastic energy with each displacement step as the cracks advance; provided the displacement increments are chosen sufficiently small. These results apply to any system of multiple cracks. This is also seen in the numerical examples. The numerical examples include evolution of a straight crack, a crack propagating inside an L-shaped domain, and two offset inward propagating cracks.

Keywords Convergence · quasistatic · Fracture · Nonlocal

D. Bhattacharya · R. Lipton (✉)
Department of Mathematics, Louisiana State University, Baton Rouge, LA 70803, USA
e-mail: lipton@lsu.edu

D. Bhattacharya
e-mail: debdeepbh@lsu.edu

P. Diehl
Center for Computation and Technology, Louisiana State University, Baton Rouge, LA 70803, USA
e-mail: pdiehl@cct.lsu.edu

1 Introduction

The hallmark of Peridynamic (PD) simulations is that dynamic fracture patterns emerge from the nonlocal model and are not prescribed (Silling 2000; Silling et al. 2007). The time evolution of the PD model is driven by temporally and spatially nonlocal forces. In this article the nonlocal forces acting between points are of cohesive type (Lipton 2014, 2016). The length scale of nonlocal interaction relative to domain size is denoted by ϵ. This length scale is referred to as the horizon as a point in the domain can only interact with other points within the horizon. Here forces between points are referred to as bonds.

In the absence of inertia one considers quasistatic or rate independent evolution. The quasistatic evolution can be unstable or correspond to an evolution over local minimizers of a nonconvex energy (Bhattacharya and Lipton 2023). This is distinct from other nonlocal methods for which evolutions are found as global minimizers of a nonconvex surface/bulk energy (Bourdin et al. 2008).

Motivated by these considerations the paper develops implicit methods to describe quasistatic fracture as an evolution over stationary points associated with local equilibria. It is clear that one can not use a linear-elastic brittle bond model in an implicit scheme since its abrupt failure leads to a discontinuity that prevents computation of the Hessian. Instead the state of the art model (Ni et al. 2018) applies the sequentially linear

analysis, where for a given load step a linear peridynamic elastic analysis is applied to find the bond with the highest stretch greater than the critical stretch. Once a linear elastic solution is found then the bond with the highest stretch is removed from the stiffness matrix and one repeats the process until no more bonds are broken. Then the load (applied force or imposed displacement) is incremented and the process is repeated until the final load is reached.

The approach developed here uses a differentiable cohesive constitutive law that is initially elastic and then softens. Because the constitutive law is differentiable a Hessian is defined and one can proceed with a well posed implicit approach. For each displacement increment we use Newton iteration to recover the local equilibrium solution of fully nonlinear PD in response to the applied displacement.

We rigorously show that the fracture evolution predicted by the model decreases stored elastic energy in the undamaged material as the cracks advance; provided the displacement increments are chosen sufficiently small. We provide a rigorous existence theory of quasistatic nonlocal fracture evolution using fixed point methods. This method is new as the fracture advances with increasing displacement increment as a result of a fixed point iteration using a smooth non-convex constitutive law.

There is now a large literature on dynamic simulations using PD, e.g., see the reviews (Bobaru et al. 2016; Javili et al. 2019; Isiet et al. 2021; Diehl et al. 2019, 2022). Building on this, dynamic relaxation methods have been applied to quasistatic PD, see for example (Kilic and Madenci 2010; Yaghoobi et al. 2017; Zhang et al. 2016; Wu et al. 2020; Mehrmashhadi et al. 2019). On the other hand, dynamic relaxation for can take numerous iterations to converge. Because of this reason, one advantage of implicit methods for quasistatic nonlocal problems is that convergence is achieved using relatively few iterations (Ni et al. 2018; Huang et al. 2015; Mikata 2012; Zaccaritto et al. 2015; Wang et al. 2019; Breitenfeld 2014; Kilic and Madenci 2010; Rabczuk and Ren 2017; Freimanis and Paeglitis 2017; Sheikhbahaei et al. 2023). Recently, several techniques to reduce the computational costs for quasistatic simulations are available. These include the adaptive use of linear elastic and peridynamic meshes (Ni et al. 2018), the fast convolution method (Jafarzadeh et al. 2022), fast Galerkin methods (Wang and Tian 2012), a multi-threaded approach for generating sparse stiffness matrices (Prakash and Stewart 2020), a combined implicit-explicit method (Hu and Madenci 2016; Hu et al. 2018), and the fire algorithm (Shiihara et al. 2019).

The nonlocal force viewed as a function of strain admits a closed-form analytical expression that is used directly to compute the Hessian. This is employed in the numerical implementation of the Newton–Raphson scheme to find the elastic displacement field and crack for each displacement step (Diehl and Lipton 2022; Bhattacharya et al. 2021), see Sect. 5.1. The shape of the force strain law can be adjusted to any analytic elastic-then-softening profile. This is done using splines or piecewise trigonometric functions. Unlike local fracture theories involving an explicit crack and elastic equilibrium equations off the crack, the nonlocal equations of equilibrium are well-defined everywhere. Here the elastic constants are determined by the slope of the force strain curve at the origon, see Eqs. (6), (7). Away from the crack the nonlocal solutions are close to local solutions of the elastic equilibrium equation. This is provably true for the nonlocal modeling of cracks in the limit of vanishing non-locality (Lipton 2014, 2016; Lipton and Jha 2021; Lipton et al. 2019). The fracture toughness of the nonlocal model introduced here is the energy per unit length required to create new surface and it is independent of horizon size (Lipton 2014, 2016), see (8). The horizon size is taken small enough to resolve flaws associated with stress concentrations according to Grifith's failure criterion (as in eqs. (21) and (22) of Diehl et al. 2016). This is illustrated in Sect. 6.3 for the L-shaped panel where no pre-crack is given and the fracture is required to nucleate from a re-entrant corner. We compare this to recent work given in Niazi et al. (2021).

Here, we prove that the fracture evolution decreases stored elastic energy with each displacement step as the cracks advance; provided the displacement increments are chosen sufficiently small, see Sect. 3. In Sect. 4, existence of nonlocal bond breaking evolution and emergence of a fracture evolution are proved. Our theoretical results in Sects. 3 and 4 are valid for any system of growing cracks.

We apply the nonlocal model to simulate the fracture evolution of a straight mode-I crack inside a square plate, capture the emergent crack growth at the re-entrant corner of an L-shaped panel as seen in experiment, and model the interaction of two inward propagating cracks as they approach each other. Nonlocal simulations show that the energy inside the undamaged

material decreases with the displacement step while cracks propagate. In earlier work Diehl et al. (2022) this constitutive model is used in a simple comparison of quasistatic damage evolution between force and displacement loading and is in line with the theory of crack resistance (Anderson 2017).

Last we point out that in this model the potentials are scaled so that the fracture toughness is independent of ϵ (see (8)). The fracture toughness of the specimen is used to calibrate the area under the force strain curve. Under this scaling the nonlocal energy density is linear elastic for small strains and independent of horizon to leading order in ϵ, see (6.104) of (Lipton 2016). see also Proposition 1 of (Silling and Lehoucq 2008). Using these features it is shown that the non-local energy converges to the Griffith fracture energy in the limit of vanishing peridynamic horizon, see (Lipton 2014, 2016; Lipton and Jha 2021; Lipton et al. 2019). The dynamic version of this model can be thought of as a nonlocal regularization of classic sharp fracture mechanics, (Lipton and Jha 2021) and (Jha and Lipton 2020).

A direct consequence of the aforementioned scaling is that the nonlocal traction conditions provably converge as $\epsilon \to 0$ to the local traction conditions of linear elasticity (Lipton and Jha 2021). In addition the elastic fields surrounding regions with broken bonds converge to linear elastic fields. The regions with broken bonds converge to time evolving cracks with zero traction conditions on the crack lips. This is theoretically shown for straight cracks in Lipton and Jha (2021). For this model the bulk elasticity constant is described by the slope of the bond force at zero strain (see (7)) and is the same everywhere in the domain. In general terms we have calibrated the "collapsed" or "$\epsilon = 0$" peridynamic elasticity tensor (Silling and Lehoucq 2008) to material properties. Because of this the peridynamic *surface effects* (Li and Bobaru 2016) are not present, this is elaborated on in the conclusion.

The paper is structured as follows: Sect. 2 introduces the nonlocal model and displacement controlled bond breaking and fracture. In Sect. 3 continuity and asymptotic energy reduction for displacement controlled fracture evolution is established. The rigorous existence theory of nonlocal fracture evolution is presented in Sect. 4. The algorithm and discretization for the implicit method is given in Sect. 5. In Sect. 6 numerical results are presented.

2 Nonlocal model and displacement controlled bond breaking and fracture

A displacement controlled fracture evolution is addressed. We provide a nonlocal mesoscopic model for quasistatic fracture. The Dirichlet data for the prescribed displacement is specified on an interaction domain Ω_d. We introduce Ω, with $\Omega_d \subset \Omega$ and the cracking body $D = \Omega \setminus \Omega_d$. The interaction domain Ω_d is of thickness equal to the length scale of nonlocal interaction ϵ. Here Ω is a bounded domain in two or three dimensions. Nonlocal interactions between a point $\mathbf{x}$ and its neighbors $\mathbf{y}$ are confined to the sphere (disk) $H_\epsilon(\mathbf{x}) = \{\mathbf{y} : |\mathbf{y} - \mathbf{x}| < \epsilon\}$. The radius ϵ is called the horizon and is chosen an order of magnitude smaller than the length scale of the domain Ω. We introduce the nonlocal strain $S(\mathbf{y}, \mathbf{x}, \mathbf{u})$ between the point $\mathbf{x}$ and any point $\mathbf{y} \in H_\epsilon(\mathbf{x})$ given by

$$S(\mathbf{y}, \mathbf{x}, \mathbf{u}) = \frac{\mathbf{u}(\mathbf{y}) - \mathbf{u}(\mathbf{x})}{|\mathbf{y} - \mathbf{x}|} \cdot \mathbf{e}_{\mathbf{y} - \mathbf{x}},$$

where $\mathbf{e}_{\mathbf{y} - \mathbf{x}}$ is the unit vector given by

$$\mathbf{e}_{\mathbf{y} - \mathbf{x}} = \frac{\mathbf{y} - \mathbf{x}}{|\mathbf{y} - \mathbf{x}|}.$$

Force is related to strain using the constitutive relation given by the cohesive force law as in Lipton (2014, 2016). Under this law the force is linear for small strains and for larger strains the force begins to soften and then approaches zero after reaching a critical strain. The force function is g' is shown in figure 1. The nonlocal force density $\mathbf{f}$ is given in terms of the nonlocal potential $\mathcal{W}(S)$ by

$$\mathbf{f}(\mathbf{y}, \mathbf{x}, \mathbf{u}) = 2\partial_S \mathcal{W}(S(\mathbf{y}, \mathbf{x}, \mathbf{u}))\mathbf{e}_{\mathbf{y} - \mathbf{x}}, \tag{1}$$

where

$$\mathcal{W}(S(\mathbf{y}, \mathbf{x}, \mathbf{u})) = \frac{J^\epsilon(|\mathbf{y} - \mathbf{x}|)}{\epsilon^{n+1}\omega_n |\mathbf{y} - \mathbf{x}|} \\ g(\sqrt{|\mathbf{y} - \mathbf{x}|}S(\mathbf{y}, \mathbf{x}, \mathbf{u})). \tag{2}$$

Here, $J^\epsilon(r) = J(\frac{r}{\epsilon})$, where J is a non-negative bounded function supported on [0, 1]. J is called the *influence function* as it determines the influence of the bond force of peridynamic neighbors $\mathbf{y}$ on the center $\mathbf{x}$

of $H_\epsilon(\mathbf{x})$. The volume of unit ball in $\mathbb{R}^n$ is denoted by ω_n.

As figure 1 illustrates, we assume that $g(r)$ and the derivatives $g'(r)$, $g''(r)$, and $g'''(r)$ are bounded for $-\infty < r < \infty$. It is required is that $g(0) = 0$ and $g(r) > 0$ otherwise, $g(r)$ together with its first three derivatives must be bounded, and that g be convex in the interval $r^e < 0 < r^c$ and concave outside this interval with finite limits $\lim_{r \to -\infty} g(r) = C^-$ and $\lim_{r \to \infty} g(r) = C^+$. Additionally $\max\{|g''(r|)\} = g''(0)$. Here we note that in the peridynamic taxonomy our cohesive model is classified as a bond-based or ordinary state based peridynamic material model outlined in Silling et al. (2007). The peridynamic force is given by

$$\mathcal{L}(\mathbf{u}) = \int_{H_\epsilon(\mathbf{x}) \cap \Omega} (\mathbf{T}(\mathbf{x})(\mathbf{y} - \mathbf{x}) - \mathbf{T}(\mathbf{y})(\mathbf{x} - \mathbf{y})) \ d\mathbf{y},$$

(3)

where

$$\mathbf{T}(\mathbf{y})(\mathbf{y} - \mathbf{x}) = \partial_S \mathcal{W}^\epsilon(S(\mathbf{y}, \mathbf{x}, \mathbf{u}(t)))\mathbf{e}_{\mathbf{y}-\mathbf{x}},$$

(4)

$$\mathbf{T}(\mathbf{x})(\mathbf{x} - \mathbf{y}) = \partial_S \mathcal{W}^\epsilon(S(\mathbf{x}, \mathbf{y}, \mathbf{u}(t)))\mathbf{e}_{\mathbf{x}-\mathbf{y}}.$$

(5)

The influence function and g are calibrated for a given material with known Lamé modulus μ and critical energy release rate G_c using the relations (Lipton 2014, 2016),

$$\mu = g''(0)/10 \int_0^1 r^3 J(r) dr, \ n = 3, ,$$

(6)

$$\mu = g''(0)/8 \int_0^1 r^2 J(r) dr, \ n = 2.$$

(7)

and

$$G_c = 2\frac{\omega_{n-1}}{\omega_n} g_\infty \int_0^1 r^n J(r) dr, \ n = 2, 3,$$

(8)

where n is the dimension and we consider plane stress for $n = 2$. In general terms we have calibrated the "collapsed" peridynamic elasticity tensor to the elastic properties of the material (Silling and Lehoucq 2008). Here we are using bond based nonlocal interactions so for plane stress $\nu = 1/3$ and in three dimensions $\nu = 1/4$ and $\lambda = \mu$ in both cases. We can also apply
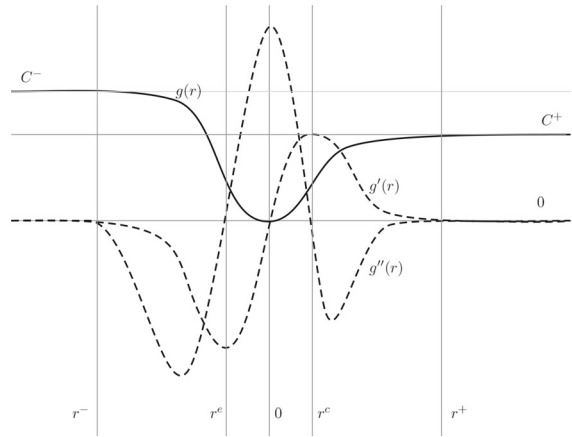

Fig. 1 The potential function $g(r)$ and derivatives $g'(r)$ and $g''(r)$ for tensile force. Here C^+ and C^- are the asymptotic values of g. The derivative of the force potential goes smoothly to zero at r^+ and r^-

more general force interactions as in state based nonlocal interactions for softening models, see (Lipton et al. 2018).

2.1 Bond breaking evolution

It is clear from figure 1 that $g''(r) \leq 0$ for

$$r^e > r = \sqrt{|\mathbf{y} - \mathbf{x}|}S(\mathbf{y}, \mathbf{x}, \mathbf{u}) \text{ or } \sqrt{|\mathbf{y} - \mathbf{x}|}S(\mathbf{y}, \mathbf{x}, \mathbf{u})$$
$$= r > r^c,$$

(9)

and we say that the bond is broken between $\mathbf{y}$ and $\mathbf{x}$ when

$$g'(\sqrt{|\mathbf{y} - \mathbf{x}|}S(\mathbf{y}, \mathbf{x}, \mathbf{u}))=0 \text{ and the strain satisfies (9)}.$$

(10)

Initially the characteristic function for all intact bonds between points $\mathbf{y} \in \Omega$ inside $H_\epsilon(\mathbf{x})$ and $\mathbf{x} \in D$ is denoted by $\chi_0(\mathbf{y}, \mathbf{x})$ and initially the whole domain is intact so $\chi_0(\mathbf{y}, \mathbf{x}) = 1$.

The nonlocal force density $\mathcal{L}_0$ is defined for all points $\mathbf{x}$ in D and $\mathbf{y}$ in Ω is given by

$$\mathcal{L}_0[\mathbf{u}](\mathbf{x}) = - \int_{H_\epsilon(\mathbf{x}) \cap \Omega} 2\chi_0(\mathbf{y}, \mathbf{x}) \frac{J^\epsilon(|\mathbf{y} - \mathbf{x}|)}{\epsilon^{n+1}\omega_n \sqrt{|\mathbf{y} - \mathbf{x}|}}$$
$$g' \left(\sqrt{|\mathbf{y} - \mathbf{x}|}S(\mathbf{y}, \mathbf{x}, \mathbf{u}) \right) \mathbf{e}_{\mathbf{y}-\mathbf{x}} d\mathbf{y}.$$

(11)

The solution to the nonlocal boundary value problem is given by a function $\mathbf{u}^1 = \mathbf{U}^1$ on Ω_d for which

$$\mathcal{L}_0[\mathbf{u}^1](\mathbf{x}) = 0, \quad \text{for } \mathbf{x} \text{ in } D. \tag{12}$$

Given the solution, $\mathbf{u}^1$ consider all pairs $(\mathbf{y}, \mathbf{x})$ with $\mathbf{y} \in \Omega$ inside $H_\epsilon(\mathbf{x})$ and $\mathbf{x} \in D$ for which the bond between them is broken. This set of pairs is called the set ΔS_1. Denote the new operator $\mathcal{L}_1(\mathbf{u})$ obtained from (11) by deleting all bond pairs in ΔS_1, let $\chi_1(\mathbf{y}, \mathbf{x})$ denote the indicator function of unbroken bonds and the solution $\mathbf{u}^1$ of (12) is also a solution of

$$\mathcal{L}_1[\mathbf{u}^1](\mathbf{x}) = 0, \quad \text{for } \mathbf{x} \text{ in } D, \tag{13}$$

where

$$\mathcal{L}_1[\mathbf{u}](\mathbf{x}) = - \int\limits_{H_\epsilon(\mathbf{x}) \cap \Omega} 2\chi_1(\mathbf{y}, \mathbf{x}) \frac{J^\epsilon(|\mathbf{y} - \mathbf{x}|)}{\epsilon^{n+1} \omega_n \sqrt{|\mathbf{y} - \mathbf{x}|}}$$
$$g'\left(\sqrt{|\mathbf{y} - \mathbf{x}|} S(\mathbf{y}, \mathbf{x}, \mathbf{u})\right) \mathbf{e}_{\mathbf{y}-\mathbf{x}} d\mathbf{y}. \tag{14}$$

Next we increment the boundary displacement to $\mathbf{U}^2$ to get the solution $\mathbf{u}^2$ of

$$\mathcal{L}_1[\mathbf{u}^2](\mathbf{x}) = 0, \quad \text{for } \mathbf{x} \text{ in } D. \tag{15}$$

where $\mathbf{u} = \mathbf{U}^2$ on Ω_d. Again given $\mathbf{u}^2$ consider all pairs $(\mathbf{y}, \mathbf{x})$ of points in $\Omega \times D \setminus \Delta S_1$ for which $|\mathbf{y} - \mathbf{x}| < \epsilon$ and the bond is broken. Call this set of pairs ΔS_2. Now set $S_1 = \Delta S_1$, and set $S_2 = S_1 \cup \Delta S_2$. Denote the new operator $\mathcal{L}_2(\mathbf{u})$ obtained from (11) by deleting bond pairs S_2 and note that the solution $\mathbf{u}^2$ of (15) is also a solution of

$$\mathcal{L}_2[\mathbf{u}^2](\mathbf{x}) = 0, \quad \text{for } \mathbf{x} \text{ in } D. \tag{16}$$

We can iterate this process with M prescribed displacements $\{\mathbf{U}^N\}_{N=1}^M$ and set $S_N = S_{N-1} \cup \Delta S_N$ to get a sequence of operators

$$\mathcal{L}_N[\mathbf{u}](\mathbf{x}) = - \int\limits_{H_\epsilon(\mathbf{x}) \cap \Omega} 2\chi_N(\mathbf{y}, \mathbf{x}) \frac{J^\epsilon(|\mathbf{y} - \mathbf{x}|)}{\epsilon^{n+1} \omega_n \sqrt{|\mathbf{y} - \mathbf{x}|}}$$
$$g'\left(\sqrt{|\mathbf{y} - \mathbf{x}|} S(\mathbf{y}, \mathbf{x}, \mathbf{u})\right) \mathbf{e}_{\mathbf{y}-\mathbf{x}} d\mathbf{y}, \tag{17}$$

solutions $\{\mathbf{u}^N\}_{N=1}^M$, and debonding sets $\{S_N\}_{N=1}^M$, with $S_1 \subset S_2 \cdots \subset S_M$. This constitutes the displacement
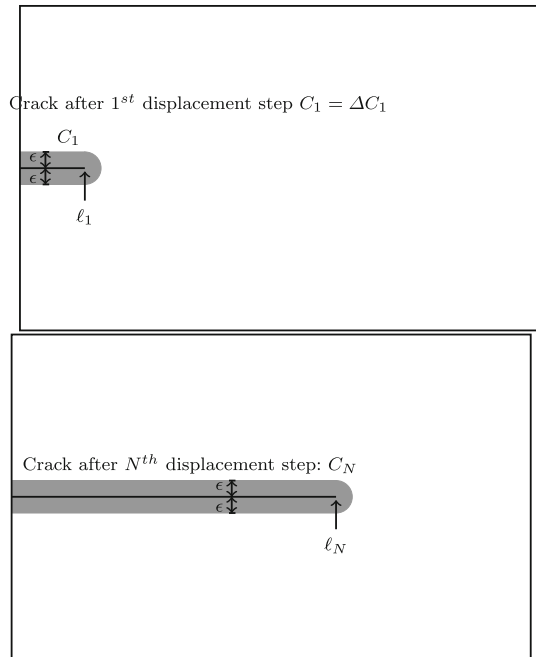

Fig. 2 The internal boundary $C_1 = \Delta C_1$ after 1st displacement step given by the line segment of length ℓ_1 after N steps it grows to length ℓ_N. The set of broken bonds for the non-local model are given by the grey regions. The set $D_0 = D$ is the interior of the rectangle, the set D_N is obtained by removing C_N at step N, see Sect. 2.2

controlled bond breaking evolution for both two and three-dimensional problems.

2.2 Fracture evolution

It is crucial to observe that in a peridynamic model crack evolution is not prescribed and only bonds between points are allowed to break. However, a bond breaking evolution can emerge that is a nonlocal fracture evolution. We now illustrate how a bond breaking evolution be can be understood as a nonlocal fracture evolution. In what follows we focus on S_1 and illustrate the ideas for the 2-dimensional problem since the three-dimensional problem is similar. Suppose the geometry of S_1 is characterized by a straight line segment ΔC_1 of length ℓ_1 across which all bonds of length less than ϵ are broken. For this case S_1 corresponds to the union of all neighborhoods that intersect ΔC_1. This is illustrated by the gray region in Fig. 2. We delete ΔC_1 from D to form the cracked region D_1 with new internal boundary $C_1 = \Delta C_1$. This kind of bond breaking geome-

try is identical to introducing a new internal boundary C_1 associated with a nonlocal traction free boundary condition. *In this way a crack appears as an internal boundary C_1 with zero nonlocal traction forces acting on either side.* So for any $\mathbf{x}$ in D, we define the set $H_\epsilon^1(\mathbf{x})$ to be all $\mathbf{y}$ in $|\mathbf{y} - \mathbf{x}| < \epsilon$ for which the bonds connecting $\mathbf{y}$ and $\mathbf{x}$ do not intersect C^1. The set $\Omega_1 = \Omega_d \cup D_1$. Here D_1 has internal boundary C_1. The operator $\mathcal{L}_1[\mathbf{u}](\mathbf{x})$ for $\mathbf{x}$ on D can now be rewritten as

$$\mathcal{L}_1[\mathbf{u}](\mathbf{x}) = - \int_{H_\epsilon^1(\mathbf{x}) \cap \Omega_1} 2 \frac{J^\epsilon(|\mathbf{y} - \mathbf{x}|)}{\epsilon^{n+1} \omega_n \sqrt{|\mathbf{y} - \mathbf{x}|}}$$
$$g'\left(\sqrt{|\mathbf{y} - \mathbf{x}|} S(\mathbf{y}, \mathbf{x}, \mathbf{u})\right) \mathbf{e}_{\mathbf{y}-\mathbf{x}} d\mathbf{y}, \qquad (18)$$

where $\mathbf{u} = \mathbf{U}^1$ on Ω_d. The nonolocal traction free boundary conditions are natural boundary conditions. They are given in (18) through the choice of the integration domain $H_\epsilon^1(\mathbf{x}) \cap \Omega_1$. More generally, one has a similar formula for $\mathcal{L}_1$ for the case when S_1 given by the collection of all bonds that intersect a smooth curve segment ΔC_1. As before, we delete the smooth curve from D to get D_1 and the formula for $\mathcal{L}_1$ given by (18). Similarly, we can suppose the same for $\Delta S_2, \ldots, \Delta S_M$ to get a growing crack $C_N = C_{N-1} \cup \Delta C_N$, with decreasing sets $D_N \subset D_{N-1} \cdots \subset D_1$, $D_N = D_{N-1} \setminus \Delta C_N$ and operators

$$\mathcal{L}_N[\mathbf{u}](\mathbf{x}) = - \int_{H_\epsilon^N(\mathbf{x}) \cap \Omega_N} 2 \frac{J^\epsilon(|\mathbf{y} - \mathbf{x}|)}{\epsilon^{n+1} \omega_n \sqrt{|\mathbf{y} - \mathbf{x}|}}$$
$$g'\left(\sqrt{|\mathbf{y} - \mathbf{x}|} S(\mathbf{y}, \mathbf{x}, \mathbf{u})\right) \mathbf{e}_{\mathbf{y}-\mathbf{x}} d\mathbf{y}, \qquad (19)$$

with $\Omega_N = \Omega_d \cup D_N$. Here D_N has internal boundary C_N and $H_\epsilon^N(\mathbf{x})$ are all $\mathbf{y}$ in $|\mathbf{y} - \mathbf{x}| < \epsilon$ for which the bonds connecting $\mathbf{y}$ and $\mathbf{x}$ do not intersect C^N. This constitutes the displacement controlled fracture evolution.

The solution $\mathbf{u}^N$ to $\mathcal{L}_N[\mathbf{u}^N] = 0$ for each displacement loading $\mathbf{U}^N$ in the fracture evolution is found numerically using the Newton–Raphson method. This is addressed in Sect. 5. The next section shows that the elastic energy stored in the intact material decreases with each displacement step when the displacement step is sufficiently small.

3 Continuity and asymptotic energy reduction for displacement controlled fracture evolution

Here, it is shown that the fracture evolution decreases stored elastic energy with each displacement step as the cracks advance; provided the displacement increments are chosen sufficiently small. This is illustrated when we work on the space of essentially bounded displacements $\mathbf{u}$ on Ω denoted by $L^\infty(\Omega, \mathbb{R}^n)$, $n = 2, 3$. It is assumed that any prescribed displacement $\mathbf{U}$ on Ω_d belongs to this space and takes the value 0 in D. This set of boundary displacements is a subspace of $L^\infty(\Omega, \mathbb{R}^n)$ and we denote it by $\mathcal{B}$. Any displacement $\mathbf{u}$ where $\mathbf{u} = \mathbf{U}$ in Ω_d can be written as $\mathbf{u} = \mathbf{v} + \mathbf{U}$ where $\mathbf{v}$ belongs to $\mathcal{V} = \{\mathbf{v} \in L^\infty(\Omega, \mathbb{R}^n), \mathbf{v} = 0 \text{ on } \Omega_d\}$ and $\mathbf{U}$ belongs to $\mathcal{B}$. Adopting standard convention one has $\mathbf{u}$ in $\mathcal{V} + \mathcal{B}$. We extend $\mathcal{L}_N[\mathbf{u}]$ by 0 for all $\mathbf{x}$ in $\Omega \setminus D$.

The operator $\mathcal{L}_N$ satisfies several properties (Bhattacharya and Lipton 2023):
The operator $\mathcal{L}_N$ is uniformly Lipschitz continuous on $L^\infty(\Omega, \mathbb{R}^n)$, i.e.,

$$\|\mathcal{L}_N[\mathbf{u} + \Delta\mathbf{u}] - \mathcal{L}_N[\mathbf{u}]\|_\infty$$
$$\leq C \|\Delta\mathbf{u}\|_\infty \text{ for } C \text{ independent of } \mathbf{u} + \Delta\mathbf{u}, \qquad (20)$$

here $||\cdot||_\infty$ is the $L^\infty(\Omega, \mathbb{R}^n)$ norm. It now follows that $\mathcal{L}_N[\mathbf{u}]$ belongs to $\mathcal{V}$ and for fixed $\mathbf{U}$ in $\mathcal{B}$ the operator $\mathcal{L}_N[\mathbf{v}]$ is a bounded operator from $\mathcal{V}$ into itself.

The operator $\mathcal{L}_N[\mathbf{u}]$ is Fréchet differentiable and is the bounded linear functional acting on $\Delta\mathbf{u} \in L^\infty(\Omega, \mathbb{R}^n)$ given by

$$\mathcal{L}_N'[\mathbf{u}]\Delta\mathbf{u} =$$
$$- \int_{H_\epsilon^N(\mathbf{x}) \cap \Omega_N} \frac{J^\epsilon(|\mathbf{y} - \mathbf{x}|)}{\epsilon^{n+1} \omega_n} g''\left(\sqrt{|\mathbf{y} - \mathbf{x}|} S(\mathbf{y}, \mathbf{x}, \mathbf{u})\right)$$
$$S(\mathbf{y}, \mathbf{x}, \Delta\mathbf{u}) \mathbf{e}_{\mathbf{y}-\mathbf{x}} d\mathbf{y}. \qquad (21)$$

The operator $\mathcal{L}_N[\mathbf{u}]$ is continuously Fréchet differentiable, i.e.,

$$\lim_{\|\Delta\mathbf{u}\|_\infty \to 0}$$
$$\frac{\|\mathcal{L}_N[\mathbf{u} + \Delta\mathbf{u}](\mathbf{x}) - \mathcal{L}_N[\mathbf{u}](\mathbf{x}) - \mathcal{L}_N'[\mathbf{u}]\Delta\mathbf{u}\|_\infty}{\|\Delta\mathbf{u}\|_\infty} = 0, \qquad (22)$$

and the derivative is Lipshitz continuous in $\mathbf{u}$, i.e., for $\boldsymbol{\delta}, \Delta\mathbf{u} \in L^\infty(\Omega, \mathbb{R}^n)$ there is a constant C independent of $\boldsymbol{\delta}$ such that

$$\frac{\|\mathcal{L}'_N[\mathbf{u} + \boldsymbol{\delta}]\Delta\mathbf{u} - \mathcal{L}'_N[\mathbf{u}]\Delta\mathbf{u}\|_\infty}{\|\Delta\mathbf{u}\|_\infty} \leq C\|\boldsymbol{\delta}\|_\infty. \qquad (23)$$

From (23) we have a K independent of $\mathbf{u} - \mathbf{w}$ in $\mathcal{B} + \mathcal{V}$ such that

$$|||\mathcal{L}'_N[\mathbf{u}] - \mathcal{L}'_N[\mathbf{w}]||| < K\|\mathbf{u} - \mathbf{w}\|_\infty \qquad (24)$$

Here $||| \cdot |||$ is the operator norm for the linear functionals defined on $L^\infty(\Omega, \mathbb{R}^n)$.

Remark 1 (Bond breaking evolution) In summary the operator $\mathcal{L}'_N$ for $\mathbf{u}$ in $\mathcal{V} + \mathcal{B}$ is given for both bond breaking and nonlocal fracture by

$$\mathcal{L}'_N[\mathbf{u}]\Delta\mathbf{u}(\mathbf{x}) =$$
$$- \int_{H_\epsilon(\mathbf{x}) \cap \Omega} \chi_N(\mathbf{y}, \mathbf{x}) \frac{J^\epsilon(|\mathbf{y} - \mathbf{x}|)}{\epsilon^{n+1}\omega_n} g'' \left(\sqrt{|\mathbf{y} - \mathbf{x}|} \right.$$
$$\left. S(\mathbf{y}, \mathbf{x}, \mathbf{u}) \right) S(\mathbf{y}, \mathbf{x}, \Delta\mathbf{u}) \mathbf{e}_{\mathbf{y}-\mathbf{x}} d\mathbf{y}, \qquad (25)$$

and properties (22) through (24) hold.

The crack domain at the Nth displacement step is C_N and the set of broken bonds is S_N. The set of broken bonds S_N is given by the grey zone in Fig. 2. We define the set of intact material by $\tilde{D}_N = D \setminus S_N$. The elastic energy density stored at a point $\mathbf{x}$ in $\tilde{D}_N$ is given by

$$W_N(\mathbf{x}, \mathbf{u}^N) = \int_{H_\epsilon(\mathbf{x}) \cap \Omega} |\mathbf{y} - \mathbf{x}| \, \mathcal{W}(\mathbf{y}, \mathbf{x}, S(\mathbf{y}, \mathbf{x}, \mathbf{u}^N)) \, d\mathbf{y}.$$

The indicator function of the set $\tilde{D}_N$ taking the value 1 inside $\tilde{D}_N$ and 0 elsewhere is denoted by $\chi_{\tilde{D}_N}(\mathbf{x})$. The elastic energy of displacement inside the intact material $\tilde{D}_N$ for prescribed boundary displacement $\mathbf{U}^N$ on Ω_d is given by

$$E_N = \int_D \chi_{\tilde{D}_N}(\mathbf{x}) \, W_N(\mathbf{x}, \mathbf{u}^N) \, d\mathbf{x}. \qquad (26)$$

Energy inequality inside undamaged material
We suppose that $\mathcal{L}'_N[\mathbf{u}^N]^{-1}$ exists and is bounded for each solution $\mathbf{u}^N$ in the fracture evolution. When there

is crack propagation, i.e., $\chi_{\tilde{D}_N} > \chi_{\tilde{D}_{N+1}}$, the elastic energy satisfies,

$$E_N > E_{N+1} + \omega_{N+1}, \qquad (27)$$

If no crack propagation $\chi_{\tilde{D}_N} = \chi_{\tilde{D}_{N+1}}$, then

$$E_N = E_{N+1} + \omega_{N+1}, \qquad (28)$$

In both cases

$$\omega_{N+1} \to 0, \text{ as } \|\mathbf{U}^{N+1} - \mathbf{U}^N\|_\infty \to 0. \qquad (29)$$

This shows that the fracture evolution decreases stored elastic energy with each displacement step as the cracks advance; provided the displacement increments are chosen sufficiently small.

One can use these arguments to recover an asymptotic statement about energy reduction. At the completion of displacement step N consider a family of displacement increments $\Delta\mathbf{U}_\ell$, $\ell = 1, 2, \ldots$ with $\|\Delta\mathbf{U}_\ell\|_\infty \to 0$ that can be be applied as the $N + 1$ displacement step. Let E_ℓ to be the elastic energy of the undamaged material corresponding the applied displacement at the $N+1$ displacement step is $\mathbf{U}^N + \Delta\mathbf{U}_\ell$, then (27), (28), and (29) imply

Asymptotic energy reduction

$$E_N \geq \limsup_{\|\Delta\mathbf{U}_\ell\|_\infty \to 0} E_\ell. \qquad (30)$$

We establish (27) and (29) noting that (28) follows. We write the difference as

$$E_N - E_{N+1} = \int_D [\chi_{\tilde{D}_N}(\mathbf{x}) - \chi_{\tilde{D}_{N+1}}(\mathbf{x})] \, W_N(\mathbf{x}, \mathbf{u}^N) \, d\mathbf{x}$$
$$+ \int_D \chi_{\tilde{D}_{N+1}}(\mathbf{x}) \, [W_N(\mathbf{x}, \mathbf{u}^N) - W_{N+1}(\mathbf{x}, \mathbf{u}^{N+1})] \, d\mathbf{x},$$

the first term is positive since $\chi_{\tilde{D}_N}(\mathbf{x}) > \chi_{\tilde{D}_{N+1}}(\mathbf{x})$ and $W_N(\mathbf{x}, \mathbf{u}^N) \geq 0$. The second term can be written as

$$\int_D \chi_{\tilde{D}_{N+1}}(\mathbf{x}) \, [W_N(\mathbf{x}, \mathbf{u}^N) - W_{N+1}(\mathbf{x}, \mathbf{u}^{N+1})] \, d\mathbf{x} = \omega_{N+1}$$

where

$$\omega_{N+1} = \int_D \chi_{\tilde{D}_{N+1}}(\mathbf{x}) \left(\int_{H_\epsilon(\mathbf{x}) \cap \Omega} \frac{J^\epsilon(|\mathbf{y} - \mathbf{x}|)}{\epsilon^{n+1}\omega_n \, |\mathbf{y} - \mathbf{x}|} \right.$$

$$\left[g(\sqrt{|\mathbf{y} - \mathbf{x}|}S(\mathbf{y}, \mathbf{x}, \mathbf{u}^N)) \right.$$
$$\left. - g(\sqrt{|\mathbf{y} - \mathbf{x}|}S(\mathbf{y}, \mathbf{x}, \mathbf{u}^N + \Delta\mathbf{u})) \right] d\mathbf{y} \bigg) d\mathbf{x},$$

Using the fundamental theorem of calculus, we have

$$\omega_{N+1} = \int_D \chi_{\tilde{D}_{N+1}}(\mathbf{x}) \int_0^1 T(\mathbf{x}, t) \, dt \, d\mathbf{x},$$

where

$$T(\mathbf{x}, t) = \int_{H_\epsilon(\mathbf{x}) \cap \Omega} \frac{J^\epsilon(|\mathbf{y} - \mathbf{x}|)}{\epsilon^{n+1}\omega_n |\mathbf{y} - \mathbf{x}|} g'\left(\sqrt{|\mathbf{y} - \mathbf{x}|}\mathbf{r}(t)\right)$$
$$\sqrt{|\mathbf{y} - \mathbf{x}|}S(\mathbf{y}, \mathbf{x}, \Delta\mathbf{u}) \, d\mathbf{y},$$

with $\mathbf{r}(t) = \sqrt{|\mathbf{y} - \mathbf{x}|}S(\mathbf{y}, \mathbf{x}, \mathbf{u}^N + t\Delta\mathbf{u})$ and $\dot{\mathbf{r}}(t) = \sqrt{|\mathbf{y} - \mathbf{x}|}S(\mathbf{y}, \mathbf{x}, \Delta\mathbf{u})$. Noting that g' is bounded and estimating as in Bhattacharya and Lipton (2023) gives

$$|T(\mathbf{x}, t)| \leq C\|\mathbf{u}^{N+1} - \mathbf{u}^N\|_\infty$$

where C will always denote a generic constant independent of $\mathbf{u}^{N+1} - \mathbf{u}^N$. From this we deduce

$$|\omega_{N+1}| \leq C\|\mathbf{u}^{N+1} - \mathbf{u}^N\|_\infty \leq C \left(\|\mathbf{v}^{N+1} - \mathbf{v}^N\|_\infty \right.$$
$$\left. + \|\mathbf{U}^{N+1} - \mathbf{U}^N\|_\infty \right). \tag{31}$$

To conclude (29) we show $\|\mathbf{v}^{N+1} - \mathbf{v}^N\|_\infty \leq C\|\mathbf{U}^{N+1} - \mathbf{U}^N\|_\infty$. Since one has that $\||\mathcal{L}'_N[\mathbf{u}^N]^{-1}\|| \leq \infty$ one sees from Banach's lemma and Lipschitz continuity (24) that there exists a closed ball $\overline{B(R, \mathbf{u}^N)} = \{\mathbf{u} : \|\mathbf{u} - \mathbf{u}^N\|_\infty \leq R\}$ of radius R and center $\mathbf{u}^N$ for which $\mathcal{L}'_N[\mathbf{u}]^{-1}$ is well defined. and consequently, a positive constant $K_N > 0$ determined at step N for which $K_N\|\mathbf{v}\|_\infty \leq \|\mathcal{L}'[\mathbf{u}]\mathbf{v}\|_\infty$ for any fixed $\mathbf{u}$ in $\overline{B(R, \mathbf{u}^N)}$ and for all $\mathbf{v} \in \mathcal{V}$. We now can choose $\|\mathbf{U}^{N+1} - \mathbf{U}^N\|_\infty$ sufficiently small so that $\mathbf{u}_0 = \mathbf{v}^N + \mathbf{U}^{N+1}$ lies inside $\mathbf{u}$ in $\overline{B(R, \mathbf{u}^N)}$.

Noting that $\mathcal{L}_N[\mathbf{u}^N] = 0$ and $\mathcal{L}_N[\mathbf{u}^{N+1}] = 0$ on D_{N+1} gives

$$A = \mathcal{L}_N[\mathbf{u}^{N+1}] - \mathcal{L}_N[\mathbf{u}_0] = \mathcal{L}_N[\mathbf{u}^N] - \mathcal{L}_N[\mathbf{u}_0] = B$$

on D_{N+1}. Here $\mathbf{u}^{N+1} - \mathbf{u}_0 = \mathbf{v}^{N+1} - \mathbf{v}^N := \Delta\mathbf{v}^{N+1}$ and $\mathbf{u}_0 - \mathbf{u}^N = \mathbf{U}^{N+1} - \mathbf{U}^N := \Delta\mathbf{U}^{N+1}$ and from the fundamental theorem of calculus as in Bhattacharya

and Lipton (2023),

$$\|A\|_\infty = \left\| \int_0^1 \mathcal{L}'_N[\mathbf{r}(t)]dt \, \Delta\mathbf{v} \right\|_\infty$$

with $\mathbf{r}(t) = \sqrt{|\mathbf{y} - \mathbf{x}|}S(\mathbf{y}, \mathbf{x}, \mathbf{u}^N + t\Delta\mathbf{v})$. From (20)

$$\|B\|_\infty \leq C \|\Delta\mathbf{U}^N\|_\infty$$

Applying the mean value theorem and calculating as in Ortega (1968) we get

$$\|A\|_\infty = \|\mathcal{L}'_N[\mathbf{r}(\bar{t})] \, \Delta\mathbf{v}\|_\infty,$$

for some $0 \leq \bar{t} \leq 1$. Since $\mathbf{r}(\bar{t})$ is in the ball $\overline{B(R, \mathbf{u}^N)}$ we get

$$K_N\|\Delta\mathbf{v}\|_\infty \leq \|A\|_\infty,$$

so

$$K_N\|\mathbf{v}^{N+1} - \mathbf{v}^N\|_\infty \leq \|A\|_\infty = \|B\|_\infty$$
$$\leq C \|\mathbf{U}^{N+1} - \mathbf{U}^N\|_\infty$$

where K_N is independent of $\|\mathbf{v}^{N+1} - \mathbf{v}^N\|_\infty$ and $\|\mathbf{U}^{N+1} - \mathbf{U}^N\|_\infty$ can be chosen small independently of K_N so (29) is established.

4 Existence of nonlocal bond breaking evolution and emergence of a fracture evolution

We begin by stating two conditions that when taken together are sufficient for the existence of an inverse of $\mathcal{L}'[\mathbf{u}]$ on $\mathcal{V}$ by showing that $\mathcal{L}'[\mathbf{u}]$ satisfies the hypotheses of (Bhattacharya and Lipton 2023, Theorem 8). One condition involves the stability tensor defined by:

Definition 1 Stability tensor

$$\mathbb{A}_N[\mathbf{u}](\mathbf{x})$$
$$= \int_{H_\epsilon^N(\mathbf{x}) \cap \Omega_N} \frac{J^\epsilon(|\mathbf{y} - \mathbf{x}|)}{\epsilon^{n+1}\omega_n|\mathbf{y} - \mathbf{x}|} g''\left(\sqrt{|\mathbf{y} - \mathbf{x}|}S(\mathbf{y}, \mathbf{x}, \mathbf{u})\right)$$
$$\mathbf{e}_{\mathbf{y}-\mathbf{x}} \otimes \mathbf{e}_{\mathbf{y}-\mathbf{x}}d\mathbf{y}. \tag{32}$$

For a fixed bases $\mathbb{A}_N[\mathbf{u}](\mathbf{x})$ is an $n \times n$ symmetric matrix, $\mathbb{A}_N[\mathbf{u}](\mathbf{x}) = \mathbb{A}_N^T[\mathbf{u}](\mathbf{x})$. We write $\mathbb{A}_N^2[\mathbf{u}] - \gamma^2\mathbb{I} > 0$ when for all $\mathbf{x} \in D$ and all $\mathbf{v} \in \mathbb{R}^n$,

$\mathbb{A}_N^2[\mathbf{u}](\mathbf{x})\mathbf{v} \cdot \mathbf{v} - \gamma^2|\mathbf{v}|^2 > 0$. The stability tensor for nonlocal modeling arises in many contexts including dynamic fracture (Silling et al. 2010; Lipton 2014; Lipton et al. 2019) and elasticity (Du et al. 2013; Mengesha and Du 2014, 2013).

To get the conditions, we set $\mathbf{u} = \mathbf{v} + \mathbf{U}$ for $\mathbf{v}$ in $\mathcal{V}$ and $\mathbf{U}$ in $\mathcal{B}$ and integrate by parts as in (Lemma 5.3 of Bhattacharya and Lipton 2023) to find that $\mathcal{L}_N'[\mathbf{u}]$ is symmetric on the $L^2(\Omega, \mathbb{R}^n)$ closure of $\mathcal{V}$. Moreover, from (Bhattacharya and Lipton 2023) we have that $\mathcal{L}_N'[\mathbf{u}]$ is a bounded operator on the $L^2(\Omega, \mathbf{R}^n)$ closure of $\mathcal{V}$. Collecting these results and applying Theorem 8 of (Bhattacharya and Lipton 2023) the sufficient conditions for an inverse are given by:

Proposition 1 (Sufficient conditions for an inverse) *Given $\mathbf{u} = \mathbf{v} + \mathbf{U}$ for boundary data $\mathbf{U}$ in $\mathcal{B}$ and $\mathbf{v}$ in $\mathcal{V}$, if $Ker\{\mathcal{L}_N'[\mathbf{u}]\} = \mathbf{0}$ for $\mathcal{L}_N'[\mathbf{u}]$ regarded as an operator on the $L^2(\Omega, \mathbb{R}^n)$ closure of $\mathcal{V}$ and if there exists $\gamma > 0$ such that $\mathbb{A}_N^2[\mathbf{u}] - \gamma^2\mathbb{I} > 0$ then $\mathcal{L}_N'[\mathbf{u}]^{-1}$ is a bounded operator on $\mathcal{V}$.*

The condition that there exists $\gamma > 0$ for which $\mathbb{A}_N^2[\mathbf{u}] - \gamma^2\mathbb{I} > 0$ is equivalent to saying that all eigenvalues of $\mathbb{A}_N[\mathbf{u}]$ lie outside an interval about 0. In Bhattacharya and Lipton (2023) it is shown that $Ker\{\mathbb{A}_N[\mathbf{u}](\mathbf{x})\} = \{\mathbf{0}\}$ on D is a necessary condition for invertibility.

Now we establish the existence of a bond breaking evolution described in Sect. 2.1 from which a fracture evolution described in Sect. 2.2 can emerge. This is done in two steps. First we prove that if the displacement $\mathbf{u}^N$ is a solution to the boundary value problem for prescribed displacement $\mathbf{U}^N$ and if it satisfies suitable hypotheses then one can find a solution $\mathbf{u}^{N+1}$ to the boundary value problem for an appropriately chosen prescribed displacement $\mathbf{U}^{N+1}$; this is the statement of Proposition 2. In the following step we establish initialization. Here we show that the evolution starts with the initial choice $\mathbf{u}^0 = 0$ and for this choice we show it is possible to apply Proposition 2, to find a solution $\mathbf{u}^1$ to the boundary value problem for an appropriately chosen prescribed displacement $\mathbf{U}^1$. To conclude we give criteria for when the evolution terminates.

Displacement increment step

We introduce a ball of radius t^* surrounding a point $\mathbf{v}^N$ in $\mathcal{V}$ given by $B(t^*, \mathbf{v}^N) = \{\mathbf{v} \in \mathcal{V} : ||\mathbf{v} - \mathbf{v}^N||_\infty < t^*\}$ and denote its closure by $\overline{B(t^*, \mathbf{v}^N)}$. Now we state the existence theorem for a displacement increment in the evolution.

Proposition 2 (Solution for displacement step $N + 1$) *Given $\mathcal{L}_N(\mathbf{u}^N) = 0$ for $\mathbf{x}$ in D and $\mathbf{u}^N = \mathbf{v}^N + \mathbf{U}^N$ with $\mathbf{v}^N$ in $\mathcal{V}$ and $\mathbf{U}^N$ in $\mathcal{B}$. If there exists $\gamma > 0$ such that $\mathbb{A}_N^2[\mathbf{u}^N] > \gamma^2\mathbb{I}$ and $Ker\{\mathcal{L}_N'[\mathbf{u}^N]\} = \mathbf{0}$ for $\mathcal{L}_N'[\mathbf{u}]$ regarded as an operator on the $L^2(\Omega, \mathbb{R}^n)$ closure of $\mathcal{V}$ then there exists a displacement $\mathbf{U}^{N+1}$ and initial deformation $\mathbf{u}_0 = \mathbf{v}^N + \mathbf{U}^{N+1}$ such that $\mathcal{L}_N'[\mathbf{u}_0]^{-1}$ exists and is a bounded linear transform on $\mathcal{V}$. Moreover there is a ball of radius t^* centered at $\mathbf{v}^N$ denoted by $B(t^*, \mathbf{v}^N)$ such the unique fixed point $\mathbf{v}^{N+1}$ of the Newton map $T(\mathbf{v}) : \overline{B(t^*, \mathbf{v}^N)} \rightarrow \overline{B(t^*, \mathbf{v}^N)}$*

$$T(\mathbf{v}) = \mathbf{v} - \mathcal{L}_N'[\mathbf{v} + \mathbf{U}^{N+1}]^{-1}\mathcal{L}_N[\mathbf{v} + \mathbf{U}^{N+1}] \quad (33)$$

belongs to the closed ball $\overline{B(t^*, \mathbf{v}^N)}$. This fixed point is isolated as there exists a radius $t^{**} > t^*$ and closed ball $\overline{B(t^{**}, \mathbf{v}^N)}$ for which no other fixed point lies. Thus, $\mathcal{L}_N[\mathbf{u}^{N+1}] = 0$ and breaking bonds according to (10) with $\mathbf{u} = \mathbf{u}^{N+1}$ delivers the new operator $\mathcal{L}_{N+1}[\mathbf{v} + \mathbf{U}]$ acting on $\mathcal{V} + \mathcal{B}$ and $\mathcal{L}_{N+1}[\mathbf{u}^{N+1}] = 0$.

We establish the proposition using the Newton-Kantorovich theorem (Kantorovich and Akilov 1964; Ortega 1968; Gragg and Tapia 1974). We have from (24) for $\mathbf{U}^{N+1}$ fixed and $\mathbf{v}$ in $\mathcal{V}$

$$|||\mathcal{L}_N'[\mathbf{v} + \mathbf{U}^{N+1}] - \mathcal{L}_N'[\mathbf{u}_0]||| < K||\mathbf{v} - \mathbf{v}^N||_\infty. \quad (34)$$

From the hypothesis of Proposition 2 and Proposition 1 we have a finite β such that

$$|||\mathcal{L}_N'[\mathbf{u}_0]^{-1}||| < \beta. \quad (35)$$

Now $\mathcal{L}_N[\mathbf{u}^N] = 0$ and from (20)

$$||\mathcal{L}_N[\mathbf{u}^N] - \mathcal{L}_N[\mathbf{u}_0]||_\infty \leq C||\mathbf{U}^{N+1} - \mathbf{U}^N||_\infty, \quad (36)$$

so we can choose $\mathbf{U}^{N+1}$ so that $||\mathbf{U}^{N+1} - \mathbf{U}^N||_\infty$ is sufficiently small so that $||\mathcal{L}_N'[\mathbf{u}_0]^{-1}\mathcal{L}_N[[\mathbf{u}_0]||_\infty \leq \eta$ with $h = \beta K \eta \leq 1/2$. Then from the Newton-Kantorovich theorem we can choose radii t^* and t^{**} such that

$$t^* = \frac{1}{\beta K}(1 - \sqrt{1 - 2h}), \qquad t^{**} = \frac{1}{\beta K}(1 + \sqrt{1 - 2h}), \quad (37)$$

and the Newton iterates converge to the unique fixed point $\mathbf{v}^{N+1}$ in the closed ball $\overline{B(t^*, \mathbf{v}^N)}$. Moreover,

$\mathcal{L}_N[\mathbf{u}^{N+1}] = 0$ and breaking bonds according to (10) with $\mathbf{u} = \mathbf{u}^{N+1}$ delivers the new operator $\mathcal{L}_{N+1}[\mathbf{v}+\mathbf{U}]$ acting on $\mathcal{V} + \mathcal{B}$ and $\mathcal{L}_{N+1}[\mathbf{u}^{N+1}] = 0$. Last, the fixed point is isolated and no other fixed points lie inside the larger closed ball $\overline{B(t^{**}, \mathbf{v}^N)}$.

Initial displacement step
We now start with the initial choice $\mathbf{u}^0 = 0$ and show that there exists a solution $\mathbf{u}^1$ to the boundary value problem for appropriate nonzero boundary data $\mathbf{U}^1$.

Proposition 3 *On choosing $\mathbf{u}^0 = 0$ we have that $\mathcal{L}'[\mathbf{u}^0]^{-1}$ exists and is a bounded linear operator mapping $\mathcal{V}$ onto $\mathcal{V}$ moreover there is a radius $R > 0$ for which $\mathbf{u}^0 = 0$ is the unique solution of the boundary value problem*

$$\mathcal{L}[\mathbf{u}^0](\mathbf{x}) = 0, \text{ for } \mathbf{x} \text{ in } D \text{ and } \mathbf{u}^0 = 0 \text{ on } \Omega_d, \quad (38)$$

among all functions in the ball $B(R, 0)$.

Proposition 3 shows that the initialization $\mathbf{u}^0 = 0$, satisfies the hypotheses of Proposition 2 so there is a least one choice of nonzero boundary displacement $\mathbf{U}^1$ for which there is a solution $\mathbf{u}^1$ of the boundary value problem (12). Breaking bonds if needed according to Proposition 2 gives the new operator $\mathcal{L}_1$ on $\mathcal{V} + \mathcal{B}$ and $\mathcal{L}_1[\mathbf{u}^1](\mathbf{x}) = 0$ for $\mathbf{x}$ in D. The proof of Proposition 3 is given in the Appendix.

Terminal displacement step
The displacement increment is terminated when $Ker\{\mathcal{L}'_{N+1}[\mathbf{u}^{N+1}]\} \neq 0$ or when $\mathbb{A}_{N+1}[\mathbf{u}^{N+1}]$ vanishes on a set of finite volume. Here it is found that $\mathcal{L}'_{N+1}[\mathbf{u}^{N+1}]^{-1}$ does not exist when the stability tensor $\mathbb{A}_{N+1}[\mathbf{u}^{N+1}](\mathbf{x})$ vanishes on a set of finite volume inside D, see (Bhattacharya and Lipton 2023).

5 Numerical algorithm for fracture evolution

It is clear that one can not use a linear-elastic brittle bond model in an implicit scheme since its abrupt failure leads to a discontinuity that prevents computation of the Hessian. Instead the state of the art implicit model applies the sequentially linear analysis (Ni et al. 2018), where for a given load step a linear peridynamic elastic analysis is applied to find the bond with the highest stretch greater than the critical stretch. The bond with the highest stretch is removed from the stiffness matrix

and one repeats until equilibrium if reached. An alternate scheme is also used where one can break several bonds at every iteration of the procedure to speed things up.

In the numerical examples given in this paper we use the softening bonds constitutive law for which the Hessian is defined. For each displacement increment we use Newton iteration to recover the equilibrium solution of fully nonlinear PD in response to the applied displacement. It is important to point out that these equilibrium solutions are local energy minima, not global minima. It is only after convergence to equilibrium that we remove fully softened bonds. In the second and third numerical examples we remove all softened bonds but again only after convergence to the PD equilibrium solution.

The solution $\mathbf{u}^N$ to $\mathcal{L}_N[\mathbf{u}^N] = 0$ for each displacement $\mathbf{U}^N$ in the fracture evolution is found numerically using the Newton-Raphson method. We prescribe an increment of boundary displacement $\Delta\mathbf{U} = \mathbf{U}^N - \mathbf{U}^{N-1}$ and starting with the initial guess $\mathbf{u}^N_0 = \mathbf{v}^{N-1} + \mathbf{U}^N$, for all k solve for $\Delta\mathbf{u}$

$$-\mathcal{L}'_{N-1}[\mathbf{u}^N_k]\Delta\mathbf{u} = \mathcal{L}_{N-1}[\mathbf{u}^N_k], \quad (39)$$

and set $\mathbf{u}^N_{k+1} = \mathbf{u}^N_k + \Delta\mathbf{u}$. The approximate root obtained after the Newton iteration $\mathbf{u}^N$ satisfies

$$\mathcal{L}_{N-1}[\mathbf{u}^N](\mathbf{x}) \approx 0, \quad (40)$$

and $\mathbf{u}^N = \mathbf{v}^N + \mathbf{U}^N = \mathbf{U}^N$ on Ω_d. Here the approximate equality "≈ 0" is measured by $||\mathcal{L}_{N-1}[\mathbf{u}^N]||_\infty \leq \tau$, with τ a preset tolerance. After reaching equilibrium we now we break all bonds for which the bond is completely softened after the Newton iteration corresponding to (10). The initial guess for the next increment $\mathbf{U}^{N+1}$ is $\mathbf{u}_0 = \mathbf{v}^N + \mathbf{U}^{N+1}$ and the process is repeated.

5.1 Discretization

Expanding $S(\mathbf{y}, \mathbf{x}, \mathbf{w}) = \frac{\mathbf{w}(\mathbf{y})-\mathbf{w}(\mathbf{x})}{|\mathbf{y}-\mathbf{x}|} \cdot \frac{\mathbf{y}-\mathbf{x}}{|\mathbf{y}-\mathbf{x}|}$ we can write

$$(L'_{N-1}[\mathbf{u}]\mathbf{w}(\mathbf{x}))_i$$
$$= \sum_{j=1}^{2} \left(\int_{H_\epsilon(\mathbf{x}) \cap \Omega_{N-1}} \sigma_{ij}(\mathbf{y}, \mathbf{x}, \mathbf{u}) w_j(\mathbf{y})d\mathbf{y} - w_j(\mathbf{x}) \right.$$

$$\left. \int\limits_{H_\epsilon(\mathbf{x}) \cap \Omega_{N-1}} \sigma_{ij}(\mathbf{y}, \mathbf{x}, \mathbf{u}) d\mathbf{y} \right) \tag{41}$$

where

$$\sigma_{ij}(\mathbf{y}, \mathbf{x}, \mathbf{u}) = \frac{J^\epsilon(|\mathbf{y} - \mathbf{x}|)}{\epsilon^{n+1} \omega_n |\mathbf{y} - \mathbf{x}|} g'' \left(\sqrt{\mathbf{y} - \mathbf{x}} S(\mathbf{y}, \mathbf{x}, \mathbf{u}) \right)$$
$$\frac{y_i - x_i}{|\mathbf{y} - \mathbf{x}|} \frac{y_j - x_j}{|\mathbf{y} - \mathbf{x}|}.$$

The domain Ω is discretized at finitely many points. Let the set of points within the interior D_{N-1} be given by $\{\mathbf{X}_i\}_{i=1}^M$. Let V_i be the volume element associated with the point $\mathbf{X}_i$. For $k = 1, \ldots, M$, denote the set of neighboring indices by $I_k^{N-1} = \{l : |\mathbf{X}_k - \mathbf{X}_l| \leq \epsilon, \ \mathbf{X}_l \in \Omega_{N-1}, \ l \neq k\}$. Define $W_i^k := w_i(\mathbf{X}_k)$ and $U_i^k := u_i(\mathbf{X}_k)$.

The discrete version of (41) is given by the linear operator $\mathbb{K}$ acting on the $2M$-dimensional vector $\mathbf{W} = \{W_i^k : i = 1, 2 \text{ and } k = 1, \ldots, M\}$ as

$$(\mathbb{K}\mathbf{W})_i^k = \sum_{j=1}^2 \sum_{l \in I_k^{N-1}} \sigma_{ij}(\mathbf{X}_l, \mathbf{X}_k, \mathbf{U}) W_j^l V_l$$
$$- \sum_{j=1}^2 W_j^k \sum_{l \in I_k^{N-1}} \sigma_{ij}(\mathbf{X}_l, \mathbf{X}_k, \mathbf{U}) V_l,$$

where the vector of nodal displacements $\mathbf{U} = \{U_i^k : i = 1, 2 \text{ and } k = 1, \ldots, M\}$.

Similarly, denoting $B_i^k := (\mathcal{L}_{N-1}[\mathbf{u}](\mathbf{X}_k))_i$ the discrete description of $\mathcal{L}_{N-1}[\mathbf{u}]$ is given by

$$B_i^k = \frac{2}{\epsilon^{n+1} \omega_n} \sum_{l \in I_k^{N-1}} \frac{J^\epsilon(|\mathbf{X}_l - \mathbf{X}_k|)}{\sqrt{|\mathbf{X}_l - \mathbf{X}_k|}} g' \left(\sqrt{|\mathbf{X}_l - \mathbf{X}_k|} \right.$$
$$\left. S(\mathbf{X}_l, \mathbf{X}_k, \mathbf{U}) \right) \frac{X_{l,i} - X_{k,i}}{|\mathbf{X}_l - \mathbf{X}_k|} V_l.$$

Solving the $2M \times 2M$ system of linear equations given by

$$-\mathbb{K}\mathbf{W} = \mathbf{B}$$

with $\mathbf{u} = \mathbf{u}_k^{N-1}$ one obtains the discretization $\mathbf{W}$ of the solution $\Delta\mathbf{u}$ to (39). The Newton iteration is terminated

with the residual $\left\| \mathcal{L}[\mathbf{u}_k^{N-1}] \right\|_\infty$ is below a prescribed tolerance.

6 Numerical examples

Here, we consider a set of numerical examples and recover stable crack growth under displacement controlled loading. We consider a straight crack growth under uniaxial tension. We observe a reduction of energy in the intact material once the cracks starts to grow. Inspired by experiment, we consider an L-shaped panel subjected to an in-plane loading. As expected, the crack starts to grow from the re-entrant corner. Finally, we consider a rectangular panel with two pre-notches with variable offsets. Under uniaxial tension, the cracks start to grow inward. The offset distance of the pre-cracks affects the interaction of the growing cracks.

In the discrete setting, the quantity *damage* is defined as

$$d(\mathbf{x}) = 1 - \frac{\text{\#intact bonds connected to } \mathbf{x}}{\text{\#total bonds connected to } \mathbf{x} \text{ in the reference configuration}}.$$

We give two types of plots for the fracture evolution. Figures 5a displays intact bonds (straight line segments) and in Figs. 5b, 8, and 10 we plot the damage d.

6.1 Material model

The force function g' is modelled using a piecewise trigonometric function ensuring continuity of g'' at zero, r_c, r_e, r_+, and r_-. For symmetry, we assume $r_e = -r_c$, $r_- = -r_+$, and $C^+ = C^-$. The potential function is therefore given by

$$g(r) = \begin{cases} C^-, & \text{if } r \leq r_- \\ \frac{N}{2} \sin(\frac{\pi(r-r_c)}{r_- - r_e}) \frac{r_- - r_e}{\pi} + \frac{M}{2} r + C_1^c, & \text{if } r_- \leq r < r_e \\ -\frac{M}{\frac{\pi}{2r_c}} \cos\left(\frac{\pi r}{2r_c}\right) + C_0^s, & \text{if } r_e \leq r \leq r_c \\ \frac{M}{2} \sin(\frac{\pi(r-r_c)}{r_+ - r_c}) \frac{r_+ - r_c}{\pi} + \frac{M}{2} r + C_0^c, & \text{if } r_c \leq r < r_+ \\ C^+, & \text{if } r \geq r_+ \end{cases}$$

where $M = \frac{C^+}{\frac{r_+ - r_c}{2} + 2\frac{r_c}{\pi}}$, $N = \frac{C^-}{\frac{r_- - r_e}{2} + 2\frac{r_e}{\pi}}$, and

$$C_0^s = \frac{2M r_c}{\pi}$$

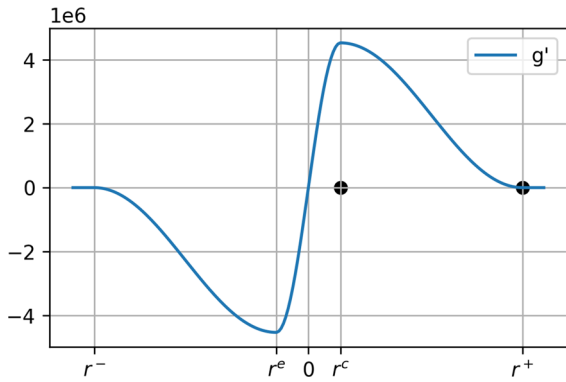$$C_0^c = M r_c \left(\frac{2}{\pi} - \frac{1}{2} \right)$$

Fig. 3 The force function g' used in Subsection 6.3. Here, $r^+ = 0.001 = -r^-$ and $r^c = 0.15r^+ = -r^e$

$$C_1^c = N r_e \left(\frac{2}{\pi} - \frac{1}{2} \right).$$

The first and second derivatives of g are given by

$$g'(r) = \begin{cases} \frac{N}{2} \cos\left(\frac{\pi(r-r_e)}{r_- - r_e} \right) + \frac{M}{2} & \text{if } r_- \leq r \leq r_c \\ M \sin\left(\frac{\pi r}{2r_c} \right), & \text{if } r_e \leq r \leq r_c \\ \frac{M}{2} \cos\left(\frac{\pi(r-r_c)}{r_+ - r_c} \right) + \frac{M}{2} & \text{if } r_c \leq r \leq r_+ \\ 0, & \text{otherwise} \end{cases}$$

and

$$g''(r) = \begin{cases} -\frac{N\pi}{2(r_- - r_e)} \sin\left(\frac{\pi(r-r_e)}{r_- - r_e} \right) + \frac{M}{2} & \text{if } r_- \leq r \leq r_- \\ \frac{M\pi}{2r_c} \cos\left(\frac{\pi}{2r_c} r \right), & \text{if } r_e \leq r \leq r_c \\ -\frac{M\pi}{2(r_+ - r_c)} \sin\left(\frac{\pi(r-r_c)}{r_+ - r_c} \right) + \frac{M}{2} & \text{if } r_c \leq r \leq r_+ \\ 0, & \text{otherwise.} \end{cases}$$

Note that, g'' continuous everywhere. The force function The force function g' associated with the material parameters described in Subsection 6.3 is shown in Fig. 3. In the following examples, we take $J \equiv 1$.

6.2 Straight crack propagation

We consider a square-shaped domain length L with a horizontal pre-notch of length $\frac{L}{4}$ on the left edge of the domain, where L = 260 mm (see Fig. 4). A regular rectangular grid is considered with meshsize $h = 2.5$ mm. The peridynamic horizon is taken to be $\epsilon = 3h$. The material parameters are taken to be $E = 210$ GPa and $G_c = 2700$ J/m^2. The domain is subjected to uniaxial
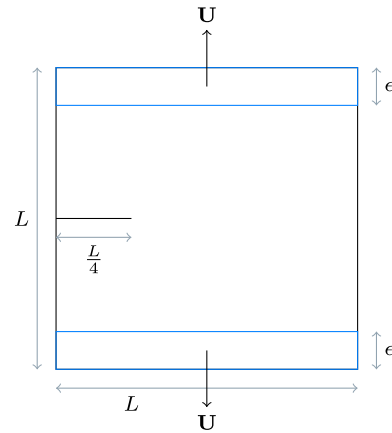

Fig. 4 Square domain with a single horizontal pre-notch

tension in the vertical direction via a displacement on the nonlocal boundary, which is taken to be a layer of thickness ϵ adjacent to the top and the bottom edge of the rectangle. We apply a vertical outward displacement of $U^0 = 2.7 \times 10^{-3}$ mm. To keep the nonlocal boundary Ω_d from experiencing damage, the bonds within Ω_d are made tougher throughout the simulation. The displacement is incremented by $\Delta U = 1.4 \times 10^{-3}$ mm at each displacement step. The crack grows at the tip of the pre-notch and extends horizontally in a straight line. Figure 5 shows the crack path evolution at displacement steps $N = 40, 70$, and 99. In the crack front, a process zone is seen where several bonds are intact. The load increment is chosen carefully so that the process zone remains the same length throughout the simulation. Beyond the process zone, all bonds are broken.

6.3 L-shaped panel test

We consider an L-shaped domain with geometry and boundary given in Fig. 6. The material parameters are chosen to be $\mu = 10.95$ GPa and $G_c = 1000$ J/m^2. The meshfree numerical approach followed here allows us to consider a non-uniform distribution of peridynamic nodes while ignoring quadrature errors when the maximum distance between the nodes is small enough. Here, an unstructured grid with 8931 nodes is used to discretize the domain. Since there is no pre-notch in the sample, we choose the strength of the material given by $\sigma_F = 24$ MPa, resulting in a peridynamic horizon of $\epsilon = 15$ mm. Here as in Diehl et al. (2016), the strength determines the horizon size and we have selected the
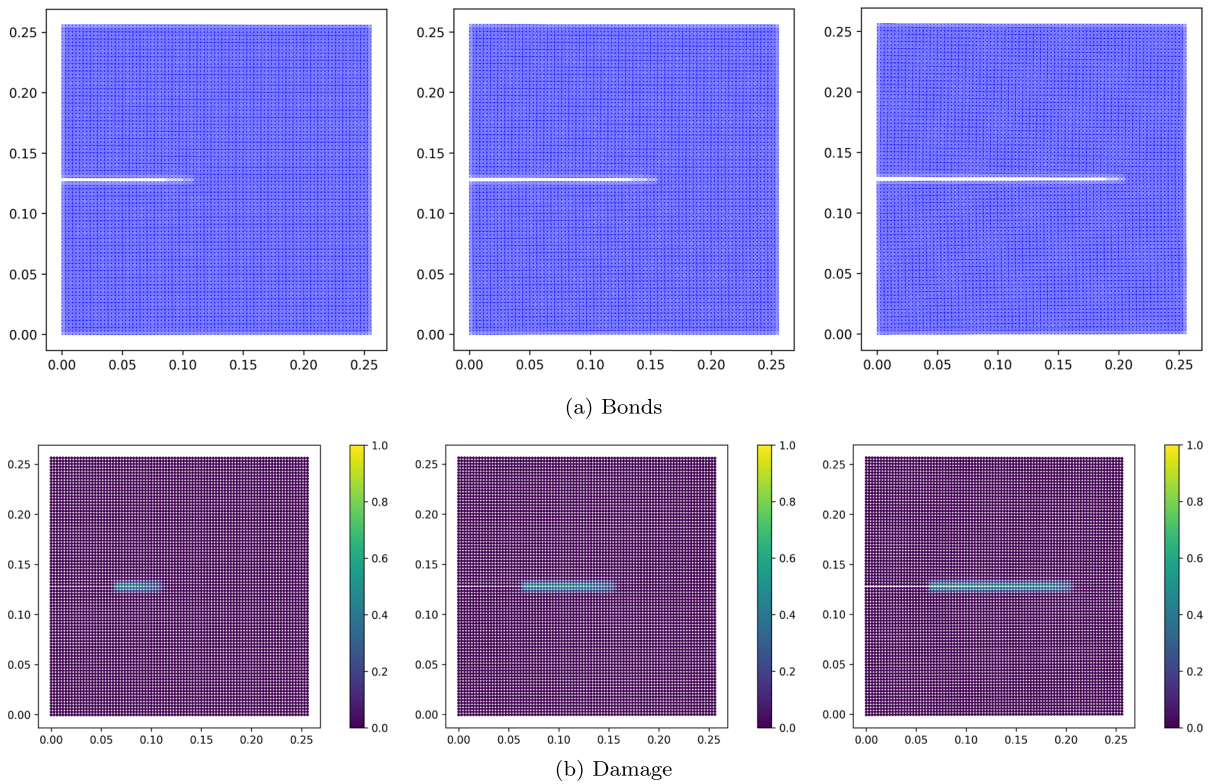
(a) Bonds

(b) Damage

Fig. 5 Straight crack propagation in a square domain

peridynamic horizon according to the Griffith's criterion given by the formula

$$\epsilon \leq \frac{G_c E}{\pi \sigma_F^2}. \tag{42}$$

This constraint on horizon size based on strength is seen to be a factor of π^2 smaller than the one developed for the bi-linear bond model in Niazi et al. (2021), in equation (17). The bottom edge of the domain is clamped while a vertical displacement is applied in the bottom-right corner of the domain. The initial displacement is taken to be $U^0 = 0.005$ mm, and it is incremented by $\Delta U = 0.00076$ mm at each displacement step. In this numerical implementation, we apply the Newton method until convergence for each displacement step. Then we break all bonds that are on the decreasing branch of the force - strain curve. Fig. 8 shows the damage for the displacement steps $N = 33, 45,$ and 56. The crack pattern is consistent with the crack pattern seen in experiment (Winkler 2001). The energy E_N with respect to the displacement step N is shown in Fig. 7a.

In Fig. 7b, we plot the residuals $\left\| \mathcal{L}[\mathbf{u}_k^N] \right\|_{L^\infty(\Omega_d)}$ associated with the Newton iteration for two different displacement steps. We plot the residual versus Newton step for a displacement step after the crack has progressed significantly (N = 88). The residuals lie below a tolerance of 10^{-10} after 4 iterations for displacement step ($N = 10$) and after 5 iterations for displacement step ($N = 88$).

6.4 Double-notched tension test

We consider a double-notched rectangular domain given in Fig. 9, which was considered in Zhao et al. (2018). The material parameters are taken to be $E = 203$ GPa and $G_c = 2700$ J/m^2. The domain is a rectangle of dimension 40 mm × 50 mm. Two horizontal pre-notches of length 10 mm are present on the left and the right edges of the rectangle. The vertical distance of the pre-notches are taken to be 0 mm, 10 mm, and 20 mm apart, respectively. A regular grid is used and the mesh size is taken to be $h = 0.5$ mm. The peridy-
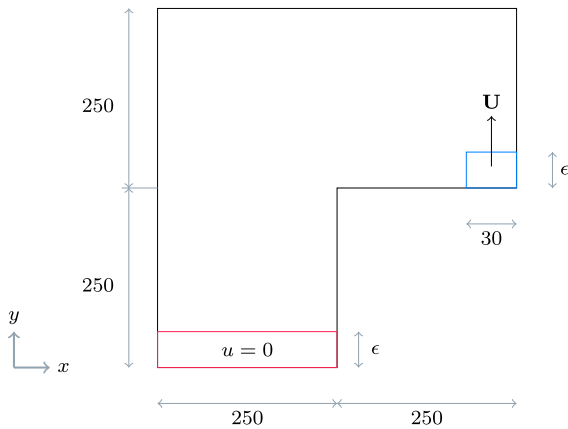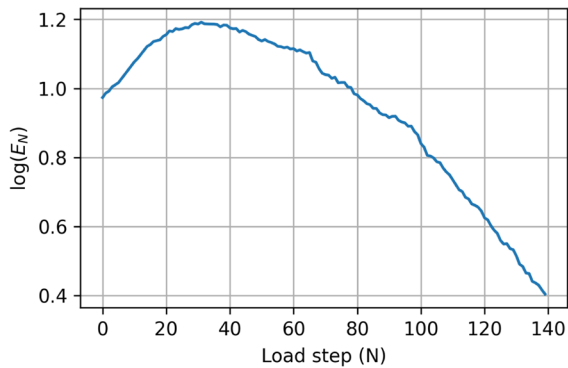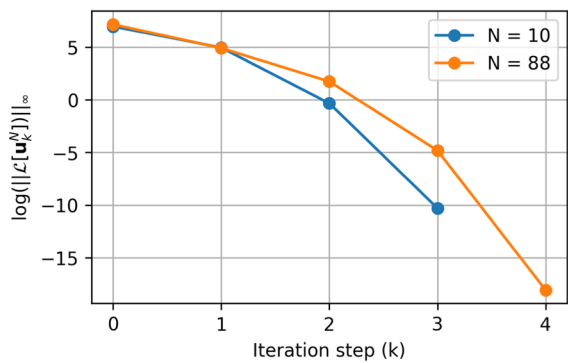
Fig. 6 L-shaped domain geometry and prescribed displacement loading

(a) Elastic energy of intact material versus the displacement step for the L-shaped panel test

(b) Residual plot to show convergence with tolerance 10^{-10} for $N = 10$ and 88

Fig. 7 L-shaped domain

namic horizon is taken to be $\epsilon = 5h$. The domain is loaded under uniaxial tension in the vertical direction. The initial applied displacement loading is taken to be

$U^0 = 9.23 \times 10^{-5}$ mm. At each displacement step N, the displacement is increased by $\Delta U = 2.4 \times 10^{-5}$ mm. In this numerical implementation, we apply the Newton method until convergence for each displacement increment. Then we break all bonds that are on the decreasing branch of the force - strain curve. The fracture patterns are shown in Fig. 10. In the domain with pre-notches with zero vertical distance, the cracks grow inward in straight lines. When the pre-notch distance is 10 mm, the cracks initially grow inward and eventually merge. When the pre-notches are too far apart (20 mm), the cracks grow inward, bend slightly toward the center, but they do not merge. The elastic energy of the intact material shown in Fig. 11.

7 Conclusion

In this paper a nonlocal quasistatic approach is developed for the evolution of multiple cracks. Using this model, a numerical method is presented and examples are given. The approach is implicit and the well-posedness of the model is proved using fixed point methods. For each displacement step it is seen that the Newton convergence of the residual as measured by the maximum norm is fast. For the straight crack it takes at most four iterations in the presence of crack growth before the residual lies below a tolerance of 10^{-5}. We have rigorously proved that the fracture evolution decreases stored elastic energy of the intact material with each displacement step as the cracks advance. This holds true theoretically provided the displacement increments are chosen sufficiently small. This is borne out in the numerical examples. The numerical examples show that crack patterns emerge from the field theory in the quasistatic context.

This paper uses the *limit calibration approach* to PD modeling developed in Lipton (2014, 2016). This approach calibrates the collapsed or "$\epsilon = 0$," PD tensor to the prescribed elastic properties of the specimen. For this choice the nonlocal model is used to solve for the emergent evolution of quasistatic fracture inside the material specimen. Here we solve a boundary value problem for the displacement inside the material. This is done for each increment in the prescribed boundary displacement. The horizon length scale is constrained to lie below the flaw length scale characterizing the material's strength and the collapsed peridynamic tensor is calibrated to the materials Young's moduli. Non-
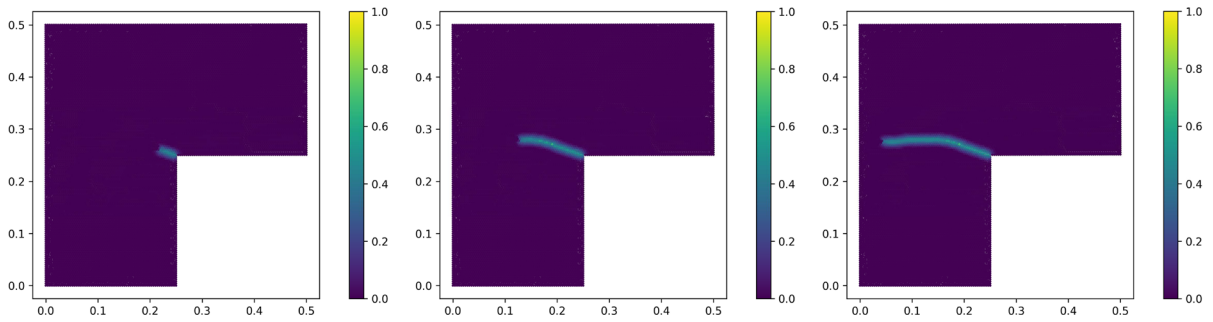
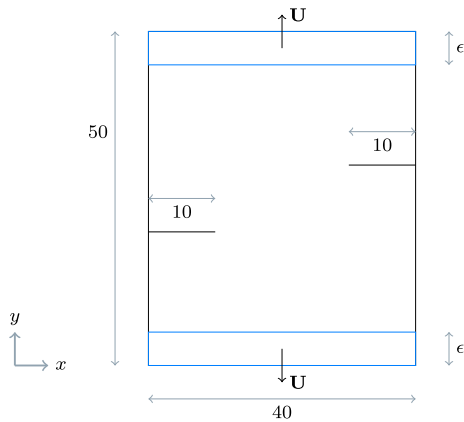**Fig. 8** Fracture in L-shaped domain: the damage plot

Fig. 9 Double-notched domain under uniaxial tension loading

local traction conditions are given on the boundary away from where the prescribed displacement increments are prescribed. The condition is described by a layer or interaction zone where no force is exerted on the center point of a neighborhood by any point within the neighborhood out side the specimen, see (Du et al. 2013). A similar condition holds for any internal boundary generated by the fracture process as outlined in Sect. 2.2. The nonlocal traction conditions provably converge as $\epsilon \to 0$ to the local traction conditions of linear elasticity (Lipton and Jha 2021). Most importantly the elastic fields surrounding internal boundaries converge to linear elastic fields. The internal boundaries converge to time evolving cracks with zero traction conditions on the crack lips. This is shown rigorously for straight cracks in Lipton and Jha (2021). For this model the bulk elasticity constant is described by the slope of the bond force at zero strain (see (7)) and is the same everywhere in the domain. In general terms we have calibrated the "collapsed" peridynamic

elasticity tensor (Silling and Lehoucq 2008) to material properties. The fracture toughness of the specimen is used to calibrate the area under the force strain curve and the PD energy Γ-converges to the Griffith fracture energy (Lipton 2014, 2016).

In a different interpretation of the model a peridynamic material is defined. Here the PD energy density associated with a fixed horizon size is calibrated to the elastic modulus of the material (Silling and Ascari 2005). When the horizon is close to the boundary its energy density decreases due to bonds crossing the specimen boundary and the calibration to material properties becomes problematic, this gives rise to the *surface effects* systematically analyzed in Li and Bobaru (2016). On the other hand in the limit calibration approach it is the nonlocal traction free conditions at external or internal boundaries that captures the effect of bonds crossing the specimen boundary.

Using the limit calibration approach we have pursued the theory further and for the dynamic model of (Lipton 2014, 2016) we surround the tip of the dynamically propagating crack with a box of finite diameter. We multiply the nonlocal equation of motion by the velocity field inside the box and integrate over the area (volume) of the box. After an integration by parts and application of Reynolds transport theorem we send the PD horizon to zero and let the diameter of the box go to zero. No assumptions are made and this procedure automatically delivers the celebrated formula relating crack tip velocity and critical energy release rate to stress intensity factor given in Freund (1972), Willis (1975). This observation and procedure was developed in Jha and Lipton (2020) and shows that the relation between crack velocity, change in internal energy and elastic energy flowing into the crack tip follows directly from
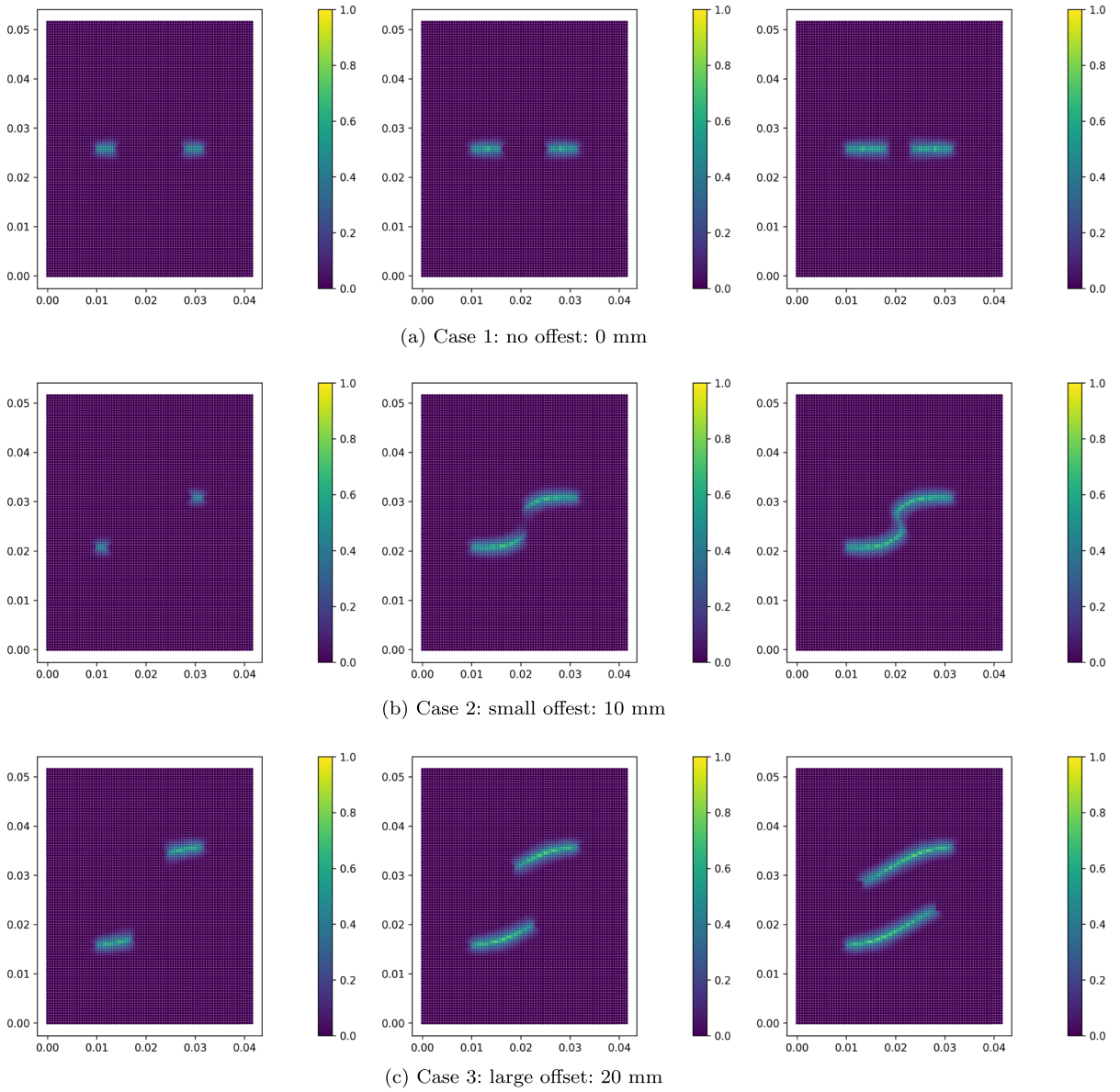
(a) Case 1: no offest: 0 mm

(b) Case 2: small offest: 10 mm

(c) Case 3: large offset: 20 mm

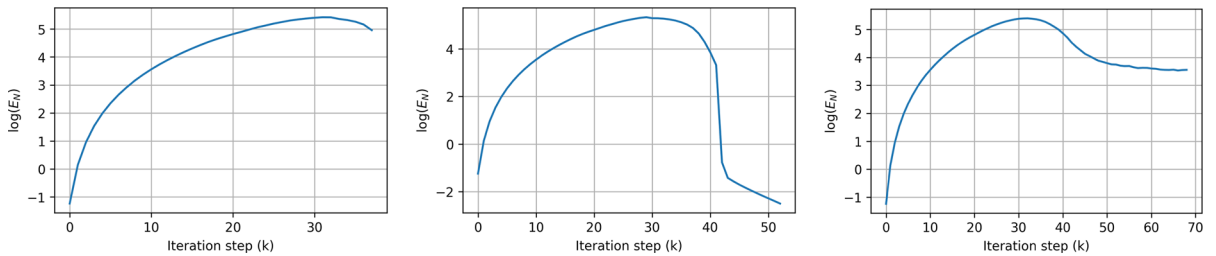**Fig. 10** Fracture patterns in double-notched tension test

Fig. 11 Elastic energy in the intact material for the double-notched tension tension with 0 mm, 10 mm, and 20 mm offset

the nonlocal model. Future work will address energy flow and energy release rate for the quasistatic case.

Appendix

We provide the proof of Proposition 3 below. Substitution of $\mathbf{u}^0 = 0$ into (25) gives

$$\mathcal{L}_0'[\mathbf{u}^0]\Delta\mathbf{u}(\mathbf{x}) = -\int_{\hat{H}_\epsilon(\mathbf{x})\cap\Omega} \frac{J^\epsilon(|\mathbf{y}-\mathbf{x}|)}{\epsilon^{n+1}\omega_n} g''(0)$$
$$S(\mathbf{y}, \mathbf{x}, \Delta\mathbf{u})\mathbf{e}_{\mathbf{y}-\mathbf{x}}d\mathbf{y}, \qquad (43)$$

and we directly verify as in Bhattacharya and Lipton (2023) that $Ker\{\mathcal{L}'[\mathbf{u}^0]\} = 0$ and $\mathbb{A}[\mathbf{u}^0] - \gamma\mathbb{I} > 0$ for some $\gamma > 0$. So $\mathcal{L}'[\mathbf{u}^0]^{-1}$ exists and is a bounded linear operator mapping $\mathcal{V}$ onto $\mathcal{V}$.

Now proceeding as in Sect. 3 we conclude there is a closed ball surrounding $\mathbf{u}^0$ given by $\overline{B(R, \mathbf{u}^0)} = \{\mathbf{u} : ||\mathbf{u} - \mathbf{u}^0||_\infty \leq R\}$ of radius $R > 0$ and center for which $\mathcal{L}_N'[\mathbf{u}]^{-1}$ is well defined. Consequently there is a positive constant $K_0 > 0$ for which $K_0||\mathbf{w}||_\infty \leq ||\mathcal{L}'[\mathbf{u}]\mathbf{w}||_\infty$ for any fixed $\mathbf{u}$ in $\overline{B(R, \mathbf{u}^0)}$ and for all $\mathbf{w} \in \mathcal{V}$. With this in hand, we now show that $\mathbf{u}^0 = 0$ is the only solution of the boundary value problem among all functions in $\overline{B(R, \mathbf{u}^0)}$. To see this suppose there is another solution $\mathbf{u}$ in $\overline{B(R, \mathbf{u}^0)}$ to the boundary value problem $\mathcal{L}[\mathbf{u}^0](\mathbf{x}) = 0$, for $\mathbf{x}$ in D and $\mathbf{u} = 0$ on Ω_d. Applying the fundamental theorem of calculus and the mean value theorem gives a $0 \leq \tilde{t} \leq 1$ for which

$$0 = ||\mathcal{L}_0[\mathbf{u}] - \mathcal{L}_0[\mathbf{u}^0]|| = ||\int_0^1 \mathcal{L}'[t\mathbf{u}]\mathbf{u}\,dt||$$
$$= ||\mathcal{L}'[\tilde{t}\mathbf{u}]\mathbf{u}|| \geq K_0||\mathbf{u}||, \qquad (44)$$

so $\mathbf{u} = 0$. Hence $\mathbf{u}^0 = 0$ is the only solution in this ball.

References

Anderson TL (2017) Fracture mechanics: fundamentals and applications. CRC Press, Boca Raton

Bhattacharya D, Lipton R (2023) Quasistatic evolution with unstable forces. Multiscale Model Simul. https://doi.org/10.1137/22M1489642

Bhattacharya D, Diehl P, Lipton RP (2021) Peridynamics for quasistatic fracture modeling. In: ASME International Mechanical Engineering Congress and Exposition, vol. 85680, p. V012T12A041. American Society of Mechanical Engineers

Bobaru F, Foster JT, Geubelle PH, Silling SA (2016) Handbook of peridynamic modeling. CRC Press, Boca Raton

Bourdin B, Francfort G, Marigo JJ (2008) The variational approach to fracture. J Elast 91:5–148

Breitenfeld M (2014) Quasi-static non-ordinary state-based peridynamics for the modeling of 3d fracture. Ph.D. thesis, University of Illinois at Urbana-Champaign, Champaign, IL

Diehl P, Lipton R (2022) Quasistatic fracture using nonlinearnonlocal elastostatics with explicit tangent stiffness matrix. Int J Numer Methods Eng 123(18):4183–4208

Diehl P, Lipton R, Schweitzer MA (2016) A numerical verification of a bond-based softening peridynamic model for small displacements: Deducing material parameters from classical linear theory. In: Institute for Numerical Simulation, Universität Bonn preprint series, vol. I.N.S. preprint 1630

Diehl P, Prudhomme S, Lévesque M (2019) A review of benchmark experiments for the validation of peridynamics models. J Peridynamics Nonlocal Model 1(1):14–35

Diehl P, Lipton R, Wick T, Tyagi M (2022) A comparative review of peridynamics and phase-field models for engineering fracture mechanics. Computational Mechanics 1–35

Du Q, Gunzburger M, Lehoucq RB, Zhou K (2013) Analysis of the volume-constrained peridynamic navier equation of linear elasticity. J Elast 113:193–217

Freimanis A, Paeglitis A (2017) Mesh sensitivity in peridynamic quasi-static simulations. Procedia Eng 172:284–291

Freund B (1972) Energy flux into the tip of an extending crack in an elastic solid. J. Elast. 2:341–349

Gragg W, Tapia R (1974) Optimal error bounds for the newton-Kantorovitch theorem. SIAM J. Numer. Anal. 11(1):10–13

Hu Y, Madenci E (2016) Bond-based peridynamic modeling of composite laminates with arbitrary fiber orientation and stacking sequence. Composite Struct 153:139–175

Hu Y, Chen H, Spencer BW, Madenci E (2018) Thermomechanical peridynamic analysis with irregular non-uniform domain discretization. Eng Fract Mech 197:92–113

Huang D, Lu G, Qiao P (2015) An improved peridynamic approach for quasi-static elastic deformation and brittle fracture analysis. Int J Mech Sci 94:111–122

Isiet M, Mišković I, Mišković S (2021) Review of peridynamic modelling of material failure and damage due to impact. Int J Impact Eng 147:103740

Jafarzadeh S, Mousavi F, Larios A, Bobaru F (2022) A general and fast convolution-based method for peridynamics: applications to elasticity and brittle fracture. Comput Methods Appl Mech Eng 392:114666

Javili A, Morasata R, Oterkus E, Oterkus S (2019) Peridynamics review. Math Mech Solids 24(11):3714–3739

Jha PK, Lipton R (2020) Kinetic relations and local energy balance for LEFM from a nonlocal peridynamic model. Int J Fract 226(1):81–95

Kantorovich L, Akilov P (1964) Functional analysis in normed spaces. Pergamon, New York

Kilic B, Madenci E (2010) An adaptive dynamic relaxation method for quasi-static simulations using the peridynamic theory. Theor Appl Fract Mech 53(3):194–204

Li Q, Bobaru F (2016) Surface corrections for peridynamic models in elasticity and fracture. Comput Mech 61:499–518

Lipton R (2014) Dynamic brittle fracture as a small horizon limit of peridynamics. J Elast 117(1):21–50

Lipton R (2016) Cohesive dynamics and brittle fracture. J Elast 124(2):143–191

Lipton RP, Jha PK (2021) Nonlocal elastodynamics and fracture. Nonlinear Differ Equ Appl. https://doi.org/10.1007/s00030-021-00683-x

Lipton R, Said E, Jha P (2018) Free damage propagation with memory. J Elast 133(2):129–153

Lipton RP, Lehoucq RB, Jha PK (2019) Complex fracture nucleation and evolution with nonlocal elastodynamics. J Peridynamics Nonlocal Model 1(2):122–130

Mehrmashhadi J, Chen Z, Zhao J, Bobaru F (2019) A stochastically homogenized peridynamic model for intraply fracture in fiber-reinforced composites. Compos Sci Technol 182:107770

Mengesha T, Du Q (2013) Analysis of a scalar nonlocal peridynamic model with a sign changing kernel. Discrete Continuous Dyn Syst B 18(5):1415–1437

Mengesha T, Du Q (2014) Nonlocal constrained value problems for a linear peridynamic Navier equation. J Elast 116(1):27–51. https://doi.org/10.1007/s10659-013-9456-z

Mikata Y (2012) Analytical solutions of peristatic and peridynamic problems for a 1d infinite rod. Int J Solids Struct 49(21):2887–2897

Ni T, Zaccariotto M, Zhu Q, Galvanetto U (2018) Static solution of crack propagation problems in peridynamics. Comput Methods Appl Mech Eng. https://doi.org/10.1016/j.cma.2018.11.028

Niazi S, Chen Z, Bobaru F (2021) Crack nucleation in brittle and quasi-brittle materials: a peridynamic analysis. Theor Appl Fract Mech 112:102855. https://doi.org/10.1016/j.tafmec.2020.102855

Ortega J (1968) The newton-kantorovich theorem. The American Math Monthly 658–660

Prakash N, Stewart RJ (2020) A multi-threaded method to assemble a sparse stiffness matrix for quasi-static solutions of linearized bond-based peridynamics. J Peridynamics Nonlocal Model 3(2):113–147

Rabczuk T, Ren H (2017) A peridynamics formulation for quasi-static fracture and contact in rock. Eng Geol 225:42–48

Sheikhbahaei P, Mossaiby F, Shojaei A (2023) An efficient peridynamic framework based on the arc-length method for fracture modeling of brittle and quasi-brittle problems with snapping instabilities. Comput Math Appl 136:165–190

Shiihara Y, Tanaka S, Yoshikawa N (2019) Fast quasi-implicit nosb peridynamic simulation based on fire algorithm. Mech Eng J

Silling SA (2000) Reformulation of elasticity theory for discontinuities and long-range forces. J Mech Phys Solids 48(1):175–209

Silling S, Ascari E (2005) A mesh free method based on the peridynamic model of solid mechanics. Comput Struct 83:1526–1536

Silling S, Lehoucq R (2008) Convergence of peridynamics to classical elasticity theory. J Elast 93:13–37

Silling SA, Epton M, Weckner O, Xu J, Askari E (2007) Peridynamic states and constitutive modeling. J Elast 88(2):151–184

Silling SA, Weckner O, Askari E, Bobaru F (2010) Crack nucleation in a peridynamic solid. Int J Fract 162(1–2):219–227

Wang H, Tian H (2012) A fast galerkin method with efficient matrix assembly and storage for a peridynamic model. J Comput Phys 231(23):7730–7738

Wang F, Ma Y, Guo Y, Huang W (2019) Studies on quasi-static and fatigue crack propagation behaviours in friction stir welded joints using peridynamic theory. Adv Mater Sci Eng

Willis J (1975) Equations of motion for propagating cracks. The Mechanics and Physics of Fracture. Met Soc 4:57–67

Winkler B (2001) Traglastuntersuchungen von unbewehrten und bewehrten Betonstrukturen auf der Grundlage eines objektiven Werkstoffgesetzes für Beton. University of Innsbruck, Austria

Wu P, Zhao J, Chen Z, Bobaru F (2020) Validation of a stochastically homogenized peridynamic model for quasi-static fracture in concrete. Eng Fract Mech 237:107293

Yaghoobi A, Chorzepa MG, Kim SS, Durham SA (2017) Mesoscale fracture analysis of multiphase cementitious composites using peridynamics. Materials 10(2):162. https://doi.org/10.3390/ma10020162

Zaccaritto M, Luongo F, Sargeo G, Galvanetto U (2015) Examples of applications of the peridynamic theory to the solution of static equilibrium problems. Aeronaut J 119:677–700

Zhang G, Le Q, Loghin A, Subramaniyan A, Bobaru F (2016) Validation of a peridynamic model for fatigue cracking. Eng Fract Mech 162:76–94

Zhao J, Tang H, Xue S (2018) Peridynamics versus xfem: a comparative study for quasi-static crack problems. Front Struct Civil Eng 12(4):548–557